Mechanical Characterization of Graphene

4

Changhong Cao, Xuezhong Wu, Xiang Xi, Tobin Filleter,
and Yu Sun

Keywords

Experimental mechanics • Graphene • Mechanical properties • Molecular dynamics simulations • Monolayer

Introduction

Graphene is a planar monolayer of strongly sp^2-bonded carbon atoms arranged into a two-dimensional honeycomb lattice with a carbon–carbon bond length of 0.142 nm [1]. It was initially assumed not to exist in free state and was described as 'academic material' [2] until 2004 when Novoselov et al. [3] successfully separated single-layer graphene experimentally. It can be wrapped up into 0D fullerenes, rolled into 1D nanotubes or stacked into 3D graphite (Fig. 4.1) [4]. Five typical methods are typically used to make graphene sheets which include [5] (i) chemical vapor deposition (CVD) on metals, (ii) micromechanical exfoliation of graphite, (iii) reduction of graphene oxide, (iv) epitaxial growth on large band gap semiconductor S_iC, (v) and the creation of colloidal suspension.

In terms of mechanical properties, graphene is a super strong nanomaterial. A suspended monolayer graphene sheet over circular holes on a Si substrate was measured by AFM (atomic force microscopy) nano-indentation revealing that it exhibits a Young's modulus of $\sim$1TPa and a critical failure stress and strain of
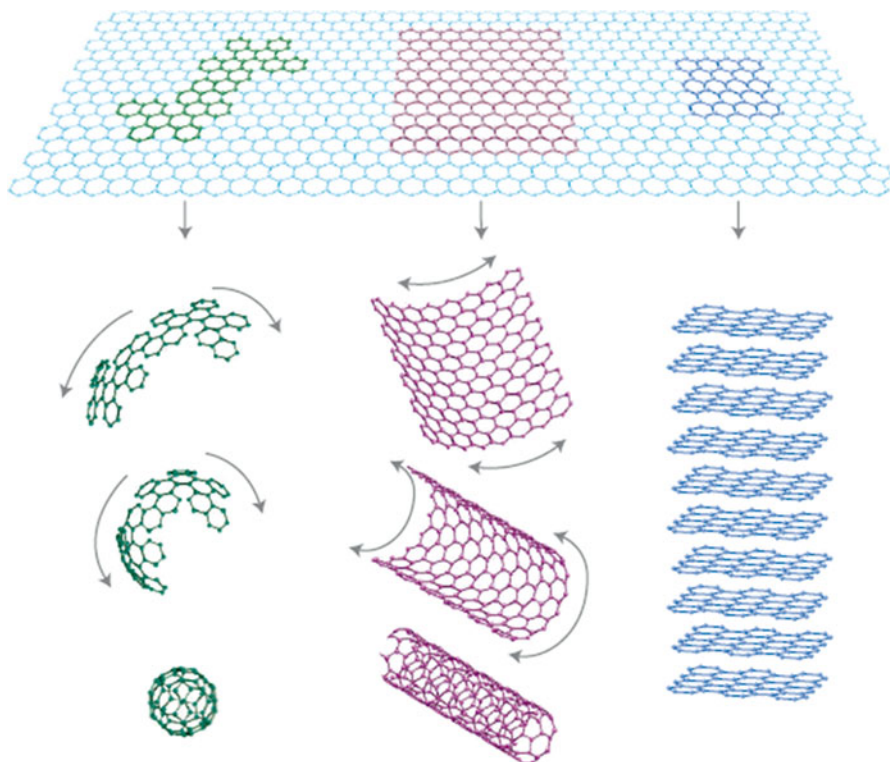
C. Cao (✉) • T. Filleter • Y. Sun

Department of Mechanical and Industrial Engineering, University of Toronto, Toronto, ON, Canada
e-mail: changhongcao@hotmail.com; filleter@mie.utoronto.ca; sun@mie.utoronto.ca

X. Wu • X. Xi

College of Mechatronics Engineering and Automation, National University of Defense Technology, Changsha, China
e-mail: www.67113@gmail.com; fordada@126.com

Fig. 4.1 Mother of all graphitic forms. Graphene is a 2D building material for carbon materials of all other dimensionalities. It can be wrapped up into 0D buckyballs, rolled into 1D nanotubes or stacked into 3D graphite (Figure/Caption reproduced (Adapted) with permission from Macmillan Publishers Ltd: [Nature Material] [4], Copyright (2007))

130GPa and 25 %, respectively [6]. These extraordinary mechanical properties, in addition to the well-documented beneficial electrical properties of graphene, have attracted a great deal of interest in areas such as nano-/microelectromechanical system (NEMS/MEMS) [7, 8], nanoelectronics [9, 10], as well as nanocomposites [11]. A detailed fundamental understanding of its mechanical properties is of importance in its application to a number of these fields, in particular nanocomposites and MEMS.

Mechanical Characterization Techniques

Optical microscopy, electron microscopy, AFM, and Raman spectroscopy have been applied to the mechanical characterization of graphene. Optical microscopy is used to image samples 'macro'scopically, and electron microscopy provides higher imaging resolutions down to nanometer and sub-nanometer scales, facilitating both structural and mechanical characterization of graphene samples. AFM is a standard

tool to obtain surface images of graphene and can also be applied in mechanical testing modes to measure mechanical properties such as Young's modulus, friction, and strength. Raman spectroscopy is used to investigate the vibrational properties of graphene and measure graphene thickness accurately, which is essential in the interpretation and analysis of graphene's mechanical behavior.

Optical microscopy is primarily used to detect graphene 'macro'scopically. Substrate design is of great importance in order to enhance the visibility of graphene under optical microscopy [12, 13]. Based on the Fabry–Perot interference mechanism, various materials have been employed to enhance imaging contrast. For example, a SiO_2 layer is usually created on the surface of a silicon substrate [14]. By adjusting the SiO_2 thickness to 90 or 300 nm, the intensity of the reflected light is at the maximum, which is also the maximum sensitivity of human eye [3]. In addition, 50 nm Si_3N_4 and 72 nm Ai_2O_3 substrates have also been used to improve the contrast of graphene [14, 15]. Additionally, fluorescence quenching microscopy (FQM) was used to image graphene, reduced graphene oxide (RGO), and graphene oxide (GO) for sample evaluation and manipulation so that the synthesis process can be improved [16].

Scanning electron microscopy (SEM) and transmission electron microscopy (TEM) are widely used in nanomaterials research. Similar to optical microscopy, an underlying substrate is needed for using SEM to image graphene sheets. The magnification of SEM is order of magnitude higher than that of optical microscopy typically achieving a spatial resolution on the order of tens to a few nms.

TEM is used to observe morphological and structural features of graphene and measure the number of graphene layers accurately. For samples in which the edges of graphene films fold back, the observation of these edges by TEM provides an accurate way to count the number of layers at multiple locations on the films, as shown in Fig. 4.2a [17]. In addition, TEM is often assisted with electron diffraction pattern analysis, which enables the observation of the crystal structure of graphene sheets [18] (Fig. 4.2b). Defects in graphene can also be detected by using this method [18]. However, it should be noted that the resolution of electron microscopy is limited by the accelerating voltage. High accelerating voltages can damage the monolayer of graphene. Aberration-corrected TEM has been reported to achieve a 1 Å resolution at an acceleration voltage of only 80 kV [19, 20].

Atomic force microscopy (AFM) can provide a direct way to observe the topography of single to few layer graphene films which are atomically thin. In theory, the thickness of a single layer of graphene is about 0.34 nm. However, due to the surface adsorption of graphene, the actual measured value consistently appears to be 0.8–1.2 nm. The number of layers can be obtained by measuring the thickness of a single-layer sheet, and it can be calculated according to [21]

$$N = \frac{P - X}{0.34} + 1$$

where N is the number of layers of graphene, P is the measured thickness, and X is the measured thickness of a single-layer graphene. Furthermore, AFM can be used
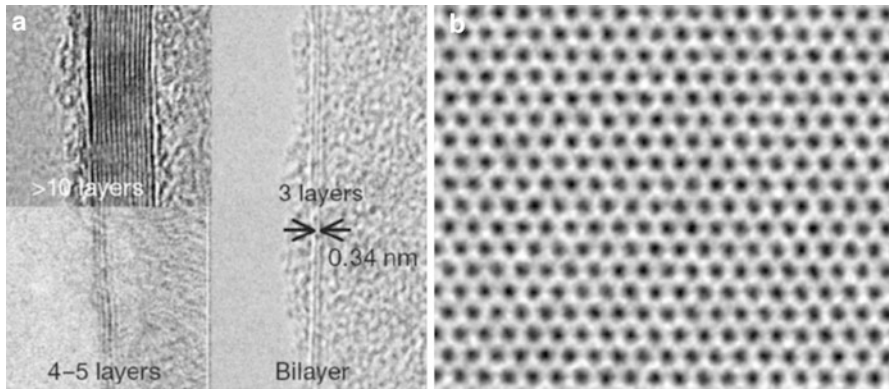
Fig. 4.2 TEM images: (**a**) Edges of graphene films (Figure/Adaption Reprinted (Adapted) by permission from Macmillan Publishers Ltd. on behalf of Cancer Research UK: [Nature] [17], Copyright (2009)) (**b**) Hexagonal pattern of the graphene structure (Figure/Caption Reprinted (adapted) with permission from [18], Copyright (2008) American Chemical Society)

to investigate the mechanical properties of graphene such as elastic modulus, tensile strength, bending stiffness, and friction. In this case, several mechanical testing modes of AFM are implemented including friction force microscopy (FFM), for determining the frictional characteristics of graphene [22–24], and AFM deflection for measuring elastic modulus and strength [6].

Raman spectroscopy provides a fast and nondestructive way to gain insight into the electron–phonon interactions in graphene. The frequency of scattered photons is changed due to the interaction of incident light and the material's molecular structure. Thus, the structural features of graphene can be identified, such as the number of graphene layers, the molecular structure, and defects in graphene [25]. Figure 4.3 shows the spectra of single-layer and double-layer graphene sheets [26]. Raman spectroscopy can also be used to measure the mechanical properties of graphene [27]. Mingyuan Huang et al. [28] presented Raman spectra of optical phonons in graphene monolayers under tunable uniaxial tensile stress. They showed that all the prominent bands exhibit significant red shifts and the resulting shift rates can be used to calibrate strain in graphene.

Mechanical Characterization of Graphene

Young's Modulus

Simulation

The elastic properties of graphene can be estimated by using numerical simulations, based on elasticity theory. It is known that graphene is a two-dimensional crystal of carbon atoms bonded by sp^2 hybridized bonds. Interatomic force field models for graphene thus can be built. Based on the continuum elasticity theory, a simple
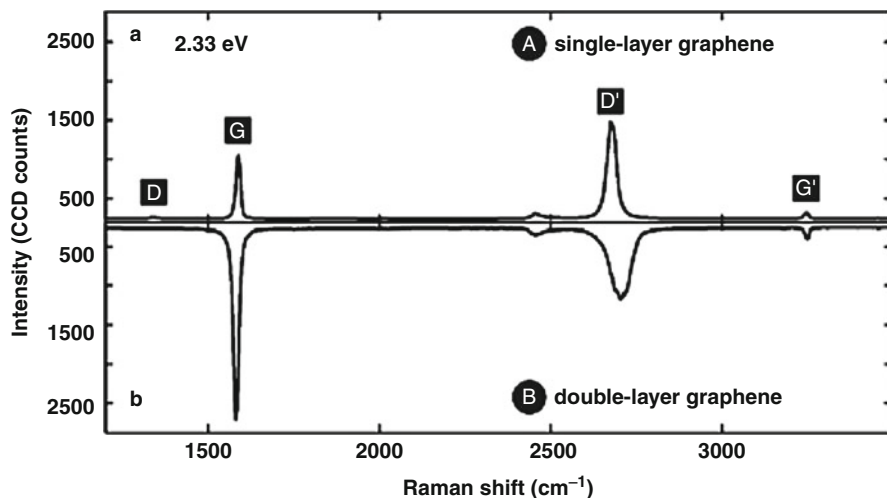
Fig. 4.3 Raman spectra of single and double layer grapheme (Figure/Caption Reprinted (adapted) with permission from [26], Copyright (2007) American Chemical Society)

Table 4.1 Graphene Young's modulus values from simulation studies

Graphene	
Study	E (TPa)
Continuum mechanics [31]	1.04
Molecular dynamics [32]	1.24
Molecular dynamics [33]	0.912
Molecular dynamics [34]	1.0913
Structural mechanics (amber model) [35]	1.305
Structural mechanics (Morse model) [35]	1.668

valence force field model was formulated by Keating [29] for semiconductors and then extended to graphene by Lobo [30]. Results predicting the Young's modulus of graphene were reported based on different modeling theories. Table 4.1 [31–35] summarizes these results from different simulation studies. It can be seen that with different modeling approaches, the Young's modulus values are close to 1 TPa.

Experiment

Reported experimental results of the Young's modulus are ∼1.0 TPa [6] which is in good agreement with simulations. A suspended monolayer graphene sheet over circular holes on a Si substrate was measured using AFM nano-indentation (Fig. 4.4) [36]. The thickness of the graphene sample was accurately determined using contact mode AFM imaging [37]. AFM was also used to accurately resolve the small forces involved in deformation and friction of graphene [36, 38]. Young's modulus is calculated according to

$$\sigma = E\varepsilon + D\varepsilon^2$$

where σ is the stress, ε is the strain, and D is the third-order elastic modulus.

Elastic properties of graphene with different boundary conditions were also measured. Wong et al. [29] investigated the mechanical properties of suspended graphene drums via static deflection experiments. Deflection was detected using AFM, which is highly sensitive to topographical changes in the out-of-plane direction and can pick up height variations as small as 1 nm. The AFM scans provided information on both the peak displacement amplitude and the deflection mode shape of the drum structure. It was found that the structures have linear spring constants ranging from 3.24 to 37.4 N m^{-1} and could be actuated to about 18–34 % of their thickness before exhibiting nonlinear deflections [29]. The result indicates a Young's modulus value of 1TPa which agrees well with the results reported by Lee et al. [6].

Bending Stiffness

Simulation

Theoretical studies have suggested that the bending stiffness of graphene is critical to attain structural stability for suspended graphene sheets, which in turn affects their mechanical properties significantly [39–41]. Molecular mechanics simulations for graphene bending rigidity were reported through calculations of the strain energy for graphene sheets subjected to a point loading [42]. Based on the first-generation Brenner potential, an analytical form was derived for the bending modulus of monolayer graphene under infinitesimal bending curvature [43, 44], namely,

Fig. 4.5 Bending rigidity variation. (**a**) Variation of the bending rigidity with the size of square graphenes; (**b**) Variation of the bending rigidity with the shape of rectangular graphenes (Figure/Caption Reprinted (Adapted) from Physics Letter A [42], Copyright (2010), with permission from Elsevier)
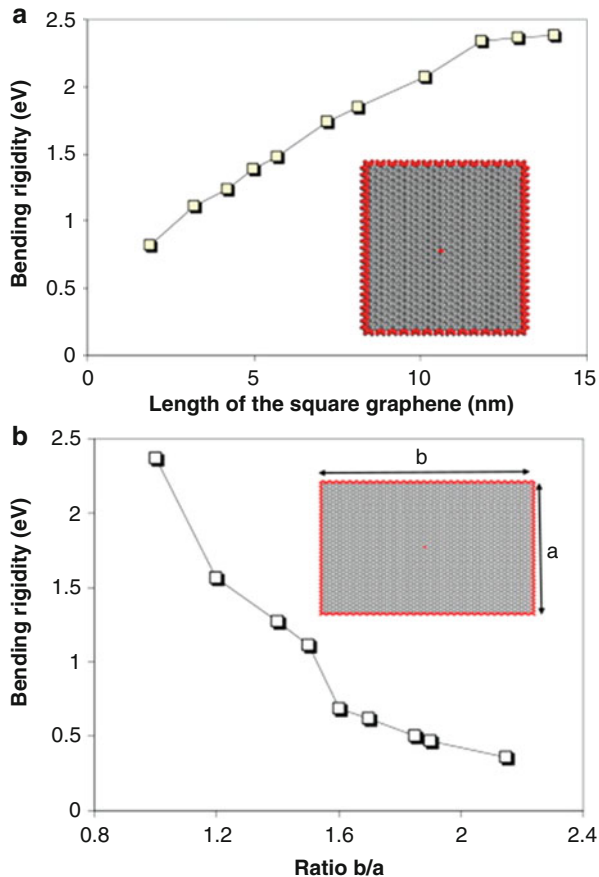

where the interatomic potential takes the form

$$V_{ij} = V_R(r_{ij}) - \overline{b}V_A(r_{ij})$$

and $\overline{b} = (b_{ij} + b_{ji})/2$ is a function of the bond angles.

Simulation results show that the bending rigidity increases from a small value of 0.819 eV with the size of 1.87 nm to an asymptotic value of 2.385 eV for sheets with sizes larger than 12 nm. In addition, rigidity changes from the asymptotic value, 2.385 eV, for a square sheet to a smaller value, 0.360 eV, for a sheet with the shape ratio of $b/a = 2.15$, as shown in Fig. 4.5 [42].
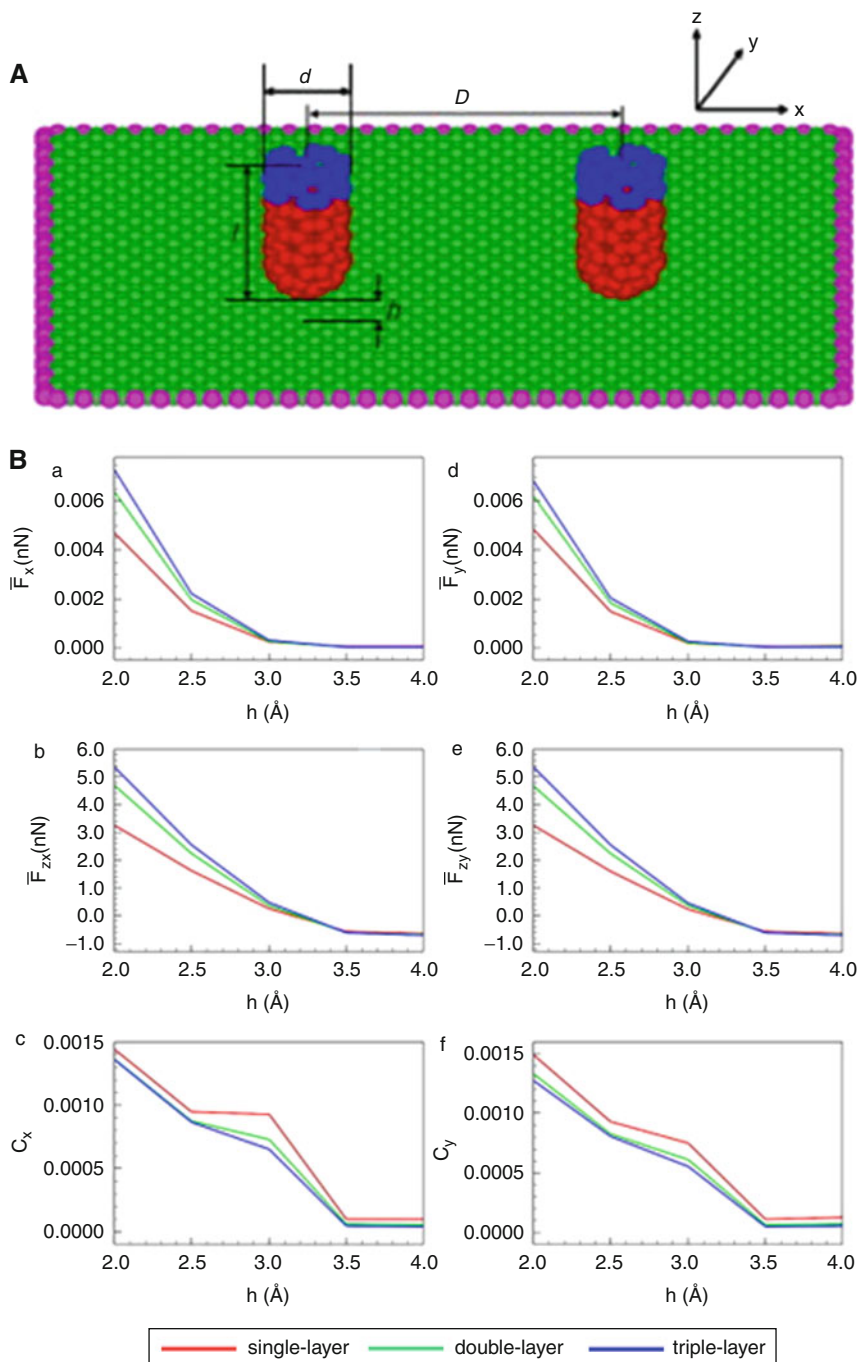
Fig. 4.6 (continued)

Experiment

While in-plane mechanical properties such as elastic modulus and strength of monolayer graphene have been deduced from experiments [6, 45], direct measurements of bending stiffness of monolayer graphene have not been reported. By using nano-indentation on suspended multilayer graphene flakes, the bending stiffness for 8–100 layers has been measured and determined to be in the range of 2×10^{-14} N m^{-2} $\times 10^{-11}$ N m^{-1} [46].

Friction

Simulation

Molecular dynamics simulations can also be applied to extract frictional properties of graphene. A probing tip using a short-capped single-walled carbon nanotube is able to capture the frictional characteristics and resolve the graphene lattice through measuring oscillatory lateral forces or normal forces. As shown in Fig. 4.6a [47], the graphene sheet (atoms are colored in red and blue) has a length l and a diameter d. The initial tip–surface distance is h, and the sliding distance is D. The atoms in blue are prescribed with a moving velocity while the atoms in red follow the molecular dynamics. The graphene sheet with lateral dimensions of 7.6×7.6 nm was placed horizontally with its boundary atoms (in pink) fixed and its interior atoms (in green) following the molecular dynamics. By averaging the oscillatory lateral force and normal force along the tip moving path, the friction coefficient was extracted [47].

Based on the simulation, it was found that the friction coefficient decreases with an increase in the initial tip–surface distance and the number of graphene layer [47]. The calculated results for the friction force $\overline{F}_x$ and the friction coefficient C_x at different initial tip–surface distances and the number of graphene layers are shown in Fig. 4.6b [47].

Experiment

The frictional properties of graphene can be measured using AFM under applied loads. Initially, the AFM tip is made to contact the specimen surface at a fixed normal load, and the friction force is measured over a distance for multiple cycles in which friction loops are recorded. Then, the applied load is varied, and the friction force is measured again for multiple applied loads. This process is repeated until the tip becomes detached from the specimen surface due to excessive negative loads and the relationship between normal force and frictional forces is determined [23, 24, 38].

Fig. 4.6 (**A**) Schematic of the probing interactions between the capped nanotube and graphene layer (**B**) Tip sliding along the x-direction, (**a**) the friction force (**c**) the friction coefficient; along the y-direction (**b**) the friction force (**d**) the friction coefficient (Figure/Caption Reprinted (Adapted) from Carbon [47], Copyright (2011), with permission from Elsevier)

Measurements down to single atomic sheets revealed that friction monotonically increased as the number of layers decreased for suspended graphene [23]; a similar trend revealed that monolayer epitaxial graphene on SiC exhibited higher friction than bilayer graphene, and the single and bilayer graphene reduced friction on the SiC substrate by a factor of $\sim$10 [24]. In another study, binding the graphene strongly to a mica surface suppressed the friction trend as a function of thickness [23, 24]. Li-Yu Lin et al. [38] investigated the friction and wear characteristics of multilayer graphene films deposited on a S_i substrate. The graphene films consisted of a few layers of carbon basal plane. The number of graphene layers was determined by AFM and Raman spectroscopy. It was found that graphene films exhibited much lower friction (from 0.36 to 0.62 nN) than bare Si surface (from 1.1 to 4.3 nN) when applied loads varied from 3 to 30 nN.

Strength and Fracture

Depending on single or polycrystalline nature, the fracture mechanisms of graphene can vary. For single crystalline graphene, the failure mechanism (take double vacancy as an example) by molecular dynamics simulation is illustrated in Fig. 4.7a [48]. Before the propagation of fracture, pentagons and heptagons initiate around the defects. As load increases, fracture disperses in the direction parallel to the loading direction. Two chains of atoms are formed at the region of the vacancy defects and the other two chains on the edges of the sheet during fracture propagation. The critical stress and critical strain relationship depends on the number of vacancy defects [48, 49]. As shown in Fig. 4.7b [48], a pristine single-layer graphene sheet has the highest ultimate strength and strain. The presence of vacancy defects can reduce these features of the graphene sheet. A single-layer graphene sheet with a single vacancy defect has a critical stress and strain reduction of 6.4 % and 9.7 %, respectively, compared with the pristine sheet. A reduction of 7.3 % and 11.46 % for a double vacancy defect graphene sheet was also estimated.

Simulation performed by Cao et al. [50] shows that for polycrystalline graphene, fracture initiates from either a grain boundary triple junction [Fig. 4.8a–d] or an array of vacancies on a preferential grain boundary [Fig. 4.8e–h] by unzipping atomic bonds along a preferential grain boundary. Crack propagation takes only 4.0 ps from crack initiation to the final failure of the entire sample. Furthermore, polycrystalline graphene exhibits 'flaw tolerance' as reported in the simulation study reported by Zhang et al. [51]. As illustrated in Fig. 4.9, fracture behavior of polycrystalline graphene can become insensitive to a preexisting flaw (hole or notch) below a critical length scale, which means that there is no stress concentration near the flaw site.

Experimental fracture behavior of graphene is relatively understudied. Research in experimentally revealing fracture mechanisms is a promising future field, which can significantly enhance the understanding of failure modes of graphene in various applications.
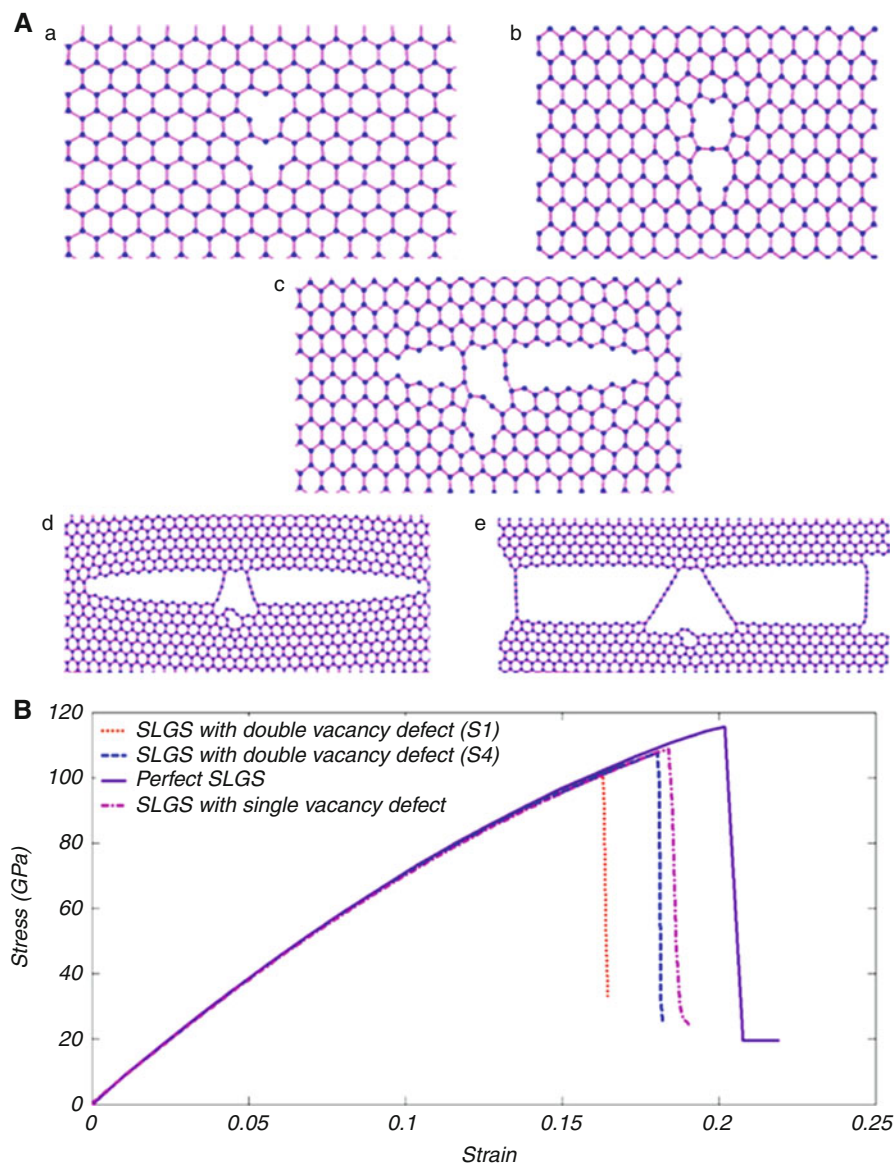
Fig. 4.7 (**A**) Failure process of a SLGS with double vacancy (shortest possible separation distance). (**a**) after initial relaxation, (**b**) formation of pentagons and heptagons at adjacent of the vacancies, (**c**) early stages of fracture propagation, (**d**) formation of two chains at the location of vacancy defects, and (**e**) formation of four chains. (**B**) Stress–strain curves of graphene sheets with double vacancies, single vacancy, and a perfect structure (Figures/Captions Reprinted (Adapted) from Solid State Communications [48], Copyright (2011), with permission from Elsevier)

Fig. 4.8 (**a–d**) Snapshots of the microstructure to show the unzipping mechanism leading to brittle inter-granular fracture. No significant out-of-plane displacement is observable. The *arrow* indicates the unzipping direction. (**e–h**) show the perforation mechanisms of separate nano-voids that cause the spontaneous initiation of crack (Figures/Captions Reprinted (Adapted) with permission from [50], Copyright [2013], American Institute of Physics)
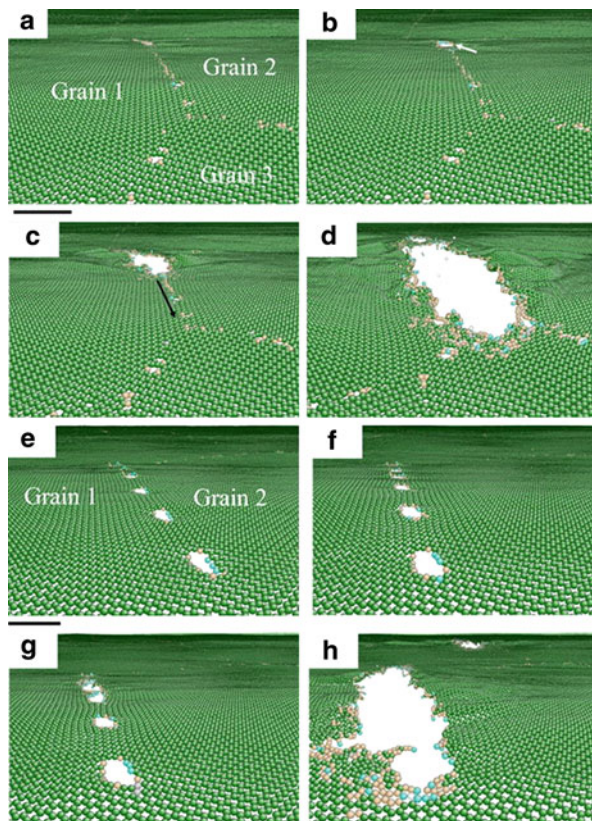
Fig. 4.9 Schematic shows the fracture behavior of the polycrystalline graphene can be insensitive to preexisting flaw (Figure/Caption Reprinted (adapted) with permission from [51], Copyright (2012) American Chemical Society)
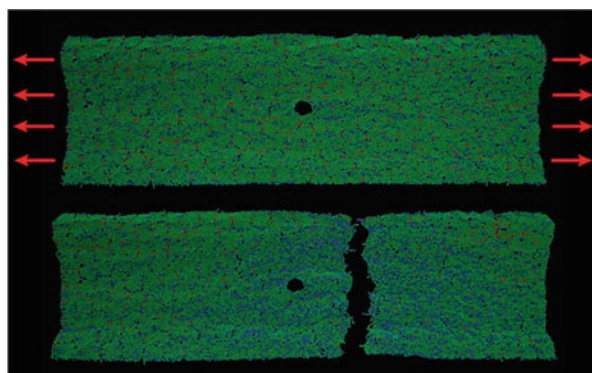
Summary

The synthesis, characterization, and applications of graphene are rapidly progressing. Mechanically, Young's modulus of mechanical exfoliated monolayer

graphene was determined to be ~1.0TPa, and a critical failure stress and strain of 130 GPa and 25 % were measured, respectively; bending stiffness was reported only for 8–100 layers to be in the range between 2×10^{-14} N m^{-1} and 2×10^{-17} N m^{-1}; friction of graphene shows a trend that it monotonically increases as the number of layers decreases for suspended graphene and epitaxial graphene on S$_i$C; fracture behavior of graphene depends on its nature of crystalline. Simulation results show that polycrystalline graphene exhibits 'flaw tolerance'. However, debates over properties such as wear and shear modulus remain unsolved. In addition to the techniques this chapter described, MEMS devices which have micrometer-sized features can also be applied to study single-layer and multilayer graphene as they can bridge investigation of materials at the macro- and nanoscales. Although a number of MEMS devices have been developed for mechanical characterizing individual 1D nanomaterials, such as carbon nanotubes [52] and silicon nanowires [53], few devices exist for characterizing 2D nanomaterials such as graphene. In future work, the development of advanced experimental techniques and methodologies for interpreting data will produce more thorough mechanical characterization results and enable additional in-depth understanding of this important nanomaterial.

References

1. Weiss PR (1958) Band structure of graphite. The State University, New Brunswick
2. Fradkin E (1986) Critical behavior of disordered degenerate semiconductors. II. Spectrum and transport properties in mean-field theory. Phys Rev B 33(5):3263–3268
3. Novoselov KS, Geim AK, Morozov SV, Jiang D, Zhang Y, Dubonos SV, Grigorieva IV, Firsov AA (2004) Electric field effect in atomically thin carbon films. Science 306(5696):666–669
4. Geim AK, Novoselov KS (2007) The rise of graphene. Nat Mater 6(3):183–191
5. Park S, Ruoff RS (2009) Chemical methods for the production of graphenes. Nat Nanotechnol 4(4):217–224
6. Lee C, Wei XD, Kysar JW, Hone J (2008) Measurement of the elastic properties and intrinsic strength of monolayer graphene. Science 321(5887):385–388
7. Yang YT, Callegari C, Feng XL, Ekinci KL, Roukes ML (2006) Zeptogram-scale nanomechanical mass sensing. Nano Lett 6(4):583–586
8. Chen CY, Rosenblatt S, Bolotin KI, Kalb W, Kim P, Kymissis I, Stormer HL, Heinz TF, Hone J (2009) Performance of monolayer graphene nanomechanical resonators with electrical readout. Nat Nanotechnol 4(12):861–867
9. Shang NG, Papakonstantinou P, McMullan M, Chu M, Stamboulis A, Potenza A, Dhesi SS, Marchetto H (2008) Catalyst-free efficient growth, orientation and biosensing properties of multilayer graphene nanoflake films with sharp edge planes. Adv Funct Mater 18(21):3506–3514
10. Thevenot DR, Toth K, Durst RA, Wilson GS (1999) Electrochemical biosensors: definitions and classification. Pure Appl Chem 71(12):16
11. Stankovich S, Dikin DA, Dommett GHB, Kohlhaas KM, Zimney EJ, Stach EA, Piner RD, Nguyen ST, Ruoff RS (2006) Graphene-based composite materials. Nature 442(7100):282–286
12. Jung I, Pelton M, Piner R, Dikin DA, Stankovich S, Watcharotone S, Hausner M, Ruoff RS (2007) Simple approach for high-contrast optical imaging and characterization of graphene-based sheets. Nano Lett 7(12):3569–3575
13. Kamat PV (2010) Graphene-based nanoarchitectures. Anchoring semiconductor and metal nanoparticles on a two-dimensional carbon support. J Phys Chem Lett 1(2):520–527

14. Blake P, Hill EW, Neto AHC, Novoselov KS, Jiang D, Yang R, Booth TJ, Geim AK (2007) Making graphene visible. Appl Phys Lett 91(6):63124

15. Gao LB, Ren WC, Li F, Cheng HM (2008) Total color difference for rapid and accurate identification of graphene. ACS Nano 2(8):1625–1633

16. Kim J, Cote LJ, Kim F, Huang JX (2010) Visualizing graphene based sheets by fluorescence quenching microscopy. J Am Chem Soc 132(1):260–267

17. Kim KS, Zhao Y, Jang H, Lee SY, Kim JM, Ahn JH, Kim P, Choi JY, Hong BH (2009) Large-scale pattern growth of graphene films for stretchable transparent electrodes. Nature 457(7230):706–710

18. Meyer JC, Kisielowski C, Erni R, Rossell MD, Crommie MF, Zettl A (2008) Direct imaging of lattice atoms and topological defects in graphene membranes. Nano Lett 8(11):3582–3586

19. Gomez-Navarro C, Meyer JC, Sundaram RS, Chuvilin A, Kurasch S, Burghard M, Kern K, Kaiser U (2010) Atomic structure of reduced graphene oxide. Nano Lett 10(4):1144–1148

20. Girit CO, Meyer JC, Erni R, Rossell MD, Kisielowski C, Yang L, Park CH, Crommie MF, Cohen ML, Louie SG, Zettl A (2009) Graphene at the edge: stability and dynamics. Science 323(5922):1705–1708

21. Dan ZH, Xu Z, Xie (2011) Graphene: structure, fabrication method and characterization. Tsinghua University Press, Beijing

22. Li QY, Lee C, Carpick RW, Hone J (2010) Substrate effect on thickness-dependent friction on graphene. Phys Status Solidi B 247(11–12):2909–2914

23. Lee C, Li QY, Kalb W, Liu XZ, Berger H, Carpick RW, Hone J (2010) Frictional characteristics of atomically thin sheets. Science 328(5974):76–80

24. Filleter T, McChesney JL, Bostwick A, Rotenberg E, Emtsev KV, Seyller T, Horn K, Bennewitz R (2009) Friction and dissipation in epitaxial graphene films. Phys Rev Lett 102(8)

25. Ferrari AC, Meyer JC, Scardaci V, Casiraghi C, Lazzeri M, Mauri F, Piscanec S, Jiang D, Novoselov KS, Roth S, Geim AK (2006) Raman spectrum of graphene and graphene layers. Phys Rev Lett 97(18)

26. Graf D, Molitor F, Ensslin K, Stampfer C, Jungen A, Hierold C, Wirtz L (2007) Spatially resolved raman spectroscopy of single- and few-layer graphene. Nano Lett 7(2):238–242

27. Gong L, Kinloch IA, Young RJ, Riaz I, Jalil R, Novoselov KS (2010) Interfacial stress transfer in a graphene monolayer nanocomposite. Adv Mater 22(24):2694–2697

28. Huang M (2009) Studies of mechanically deformed single wall carbon nanotubes and graphene by optical spectroscopy. Columbia University

29. Wong CL, Annamalai M, Wang ZQ, Palaniapan M (2010) Characterization of nanomechanical graphene drum structures. J Micromech Microeng 20(11)

30. Kysar JW (2008) Direct comparison between experiments and computations at the atomic length scale: a case study of graphene. Sci Model Simul 15(1–3):143–157

31. Shokrieh MM, Rafiee R (2010) Prediction of Young's modulus of graphene sheets and carbon nanotubes using nanoscale continuum mechanics approach. Mater Des 31(2):790–795

32. Bu H, Chen Y, Zou M, Yi H, Bi K, Ni Z (2009) Atomistic simulations of mechanical properties of graphene nanoribbons. Phys Lett A Gen, At Solid State Phys 373(37):3359–3362

33. Tsai JL, Tu JF (2010) Characterizing mechanical properties of graphite using molecular dynamics simulation. Mater Des 31(1):194–199

34. Ni Z, Bu H, Zou M, Yi H, Bi K, Chen Y (2010) Anisotropic mechanical properties of graphene sheets from molecular dynamics. Phys B Condens Matter 405(5):1301–1306

35. Scarpa F, Adhikari S, Srikantha Phani A (2009) Effective elastic mechanical properties of single layer graphene sheets. Nanotechnology 20(6)

36. Lee C, Wei XD, Li QY, Carpick R, Kysar JW, Hone J (2009) Elastic and frictional properties of graphene. Phys Status Solidi B Basic Solid State Phys 246(11–12):2562–2567

37. Nemes-Incze P, Osvath Z, Kamaras K, Biro LP (2008) Anomalies in thickness measurements of graphene and few layer graphite crystals by tapping mode atomic force microscopy. Carbon 46(11):1435–1442

38. Jun L-YL, Dae-Eun K, Whan-Kyun K, Seong C (2011) Friction and wear characteristics of multi-layer graphene films investigated by atomic force microscopy. Surf Coat Technol 205:6

39. Fasolino A, Los JH, Katsnelson MI (2007) Intrinsic ripples in graphene. Nat Mater 6(11):858–861

40. Abedpour N, Neek-Amal M, Asgari R, Shahbazi F, Nafari N, Tabar MRR (2007) Roughness of undoped graphene and its short-range induced gauge field. Phys Rev B 76(19)

41. Kim EA, Neto AHC (2008) Graphene as an electronic membrane. EPL 84(5)

42. Wang Q (2010) Simulations of the bending rigidity of graphene. Phys Lett A 374(9):1180–1183

43. Arroyo M, Belytschko T (2004) Finite crystal elasticity of carbon nanotubes based on the exponential Cauchy-Born rule. Phys Rev B 69(11)

44. Huang Y, Wu J, Hwang KC (2006) Thickness of graphene and single-wall carbon nanotubes. Phys Rev B 74(24)

45. Bunch JS, Verbridge SS, Alden JS, van der Zande AM, Parpia JM, Craighead HG, McEuen PL (2008) Impermeable atomic membranes from graphene sheets. Nano Lett 8(8):2458–2462

46. Cranford SW, Buehler MJ (2011) Packing efficiency and accessible surface area of crumpled graphene. Phys Rev B 84(20)

47. Liu P, Zhang YW (2011) A theoretical analysis of frictional and defect characteristics of graphene probed by a capped single-walled carbon nanotube. Carbon 49(11):3687–3697

48. Ansari R, Motevalli B, Montazeri A, Ajori S (2011) Fracture analysis of monolayer graphene sheets with double vacancy defects via MD simulation. Solid State Commun 151(17):1141–1146

49. Khare R, Mielke SL, Paci JT, Zhang SL, Ballarini R, Schatz GC, Belytschko T (2007) Coupled quantum mechanical/molecular mechanical modeling of the fracture of defective carbon nanotubes and graphene sheets. Phys Rev B 75(7)

50. Cao A, Qu J (2013) Atomistic simulation study of brittle failure in nanocrystalline graphene under uniaxial tension. Appl Phys Lett 102(7)

51. Zhang T, Li XY, Kadkhodaei S, Gao HJ (2012) Flaw insensitive fracture in nanocrystalline graphene. Nano Lett 12(9):4605–4610

52. Espinosa HD, Bernal RA, Filleter T (2012) In situ TEM electromechanical testing of nanowires and nanotubes. Small 8(21):3233–3252

53. Yong Z, Xinyu L, Changhai R, Yan Liang Z, Lixin D, Yu S (2011) Piezoresistivity characterization of synthetic silicon nanowires using a MEMS device. J Microelectromech Syst 20(4):959–967